Fermilab FERMILAB-PUB-06-056-E CDF

Measurement of the B_c^+ Meson Lifetime Using $B_c^+ \to J/\psi e^+ \nu_e$

A. Abulencia,[23] D. Acosta,[17] J. Adelman,[13] T. Affolder,[10] T. Akimoto,[55] M.G. Albrow,[16] D. Ambrose,[16] S. Amerio,[43] D. Amidei,[34] A. Anastassov,[52] K. Anikeev,[16] A. Annovi,[18] J. Antos,[1] M. Aoki,[55] G. Apollinari,[16] J.-F. Arguin,[33] T. Arisawa,[57] A. Artikov,[14] W. Ashmanskas,[16] A. Attal,[8] F. Azfar,[42] P. Azzi-Bacchetta,[43] P. Azzurri,[46] N. Bacchetta,[43] H. Bachacou,[28] W. Badgett,[16] A. Barbaro-Galtieri,[28] V.E. Barnes,[48] B.A. Barnett,[24] S. Baroiant,[7] V. Bartsch,[30] G. Bauer,[32] F. Bedeschi,[46] S. Behari,[24] S. Belforte,[54] G. Bellettini,[46] J. Bellinger,[59] A. Belloni,[32] E. Ben Haim,[44] D. Benjamin,[15] A. Beretvas,[16] J. Beringer,[28] T. Berry,[29] A. Bhatti,[50] M. Binkley,[16] D. Bisello,[43] R. E. Blair,[2] C. Blocker,[6] B. Blumenfeld,[24] A. Bocci,[15] A. Bodek,[49] V. Boisvert,[49] G. Bolla,[48] A. Bolshov,[32] D. Bortoletto,[48] J. Boudreau,[47] A. Boveia,[10] B. Brau,[10] C. Bromberg,[35] E. Brubaker,[13] J. Budagov,[14] H.S. Budd,[49] S. Budd,[23] K. Burkett,[16] G. Busetto,[43] P. Bussey,[20] K. L. Byrum,[2] S. Cabrera,[15] M. Campanelli,[19] M. Campbell,[34] F. Canelli,[8] A. Canepa,[48] D. Carlsmith,[59] R. Carosi,[46] S. Carron,[15] M. Casarsa,[54] A. Castro,[5] P. Catastini,[46] D. Cauz,[54] M. Cavalli-Sforza,[3] A. Cerri,[28] L. Cerrito,[42] S.H. Chang,[27] J. Chapman,[34] Y.C. Chen,[1] M. Chertok,[7] G. Chiarelli,[46] G. Chlachidze,[14] F. Chlebana,[16] I. Cho,[27] K. Cho,[27] D. Chokheli,[14] J.P. Chou,[21] P.H. Chu,[23] S.H. Chuang,[59] K. Chung,[12] W.H. Chung,[59] Y.S. Chung,[49] M. Ciljak,[46] C.I. Ciobanu,[23] M.A. Ciocci,[46] A. Clark,[19] D. Clark,[6] M. Coca,[15] G. Compostella,[43] M.E. Convery,[50] J. Conway,[7] B. Cooper,[30] K. Copic,[34] M. Cordelli,[18] G. Cortiana,[43] F. Cresciolo,[46] A. Cruz,[17] C. Cuenca Almenar,[7] J. Cuevas,[11] R. Culbertson,[16] D. Cyr,[59] S. DaRonco,[43] S. D'Auria,[20] M. D'Onofrio,[3] D. Dagenhart,[6] P. de Barbaro,[49] S. De Cecco,[51] A. Deisher,[28] G. De Lentdecker,[49] M. Dell'Orso,[46] F. Delli Paoli,[43] S. Demers,[49] L. Demortier,[50] J. Deng,[15] M. Deninno,[5] D. De Pedis,[51] P.F. Derwent,[16] T. Devlin,[52] C. Dionisi,[51] J.R. Dittmann,[4] P. DiTuro,[52] C. Dörr,[25] S. Donati,[46] M. Donega,[19] P. Dong,[8] J. Donini,[43] T. Dorigo,[43] S. Dube,[52] K. Ebina,[57] J. Efron,[39] J. Ehlers,[19] R. Erbacher,[7] D. Errede,[23] S. Errede,[23] R. Eusebi,[16] H.C. Fang,[28] S. Farrington,[29] I. Fedorko,[46] W.T. Fedorko,[13] R.G. Feild,[60] M. Feindt,[25] J.P. Fernandez,[31] R. Field,[17] G. Flanagan,[48] L.R. Flores-Castillo,[47] A. Foland,[21] S. Forrester,[7] G.W. Foster,[16] M. Franklin,[21] J.C. Freeman,[28] I. Furic,[13] M. Gallinaro,[50] J. Galyardt,[12] J.E. Garcia,[46] M. Garcia Sciveres,[28] A.F. Garfinkel,[48] C. Gay,[60]

H. Gerberich,[23] D. Gerdes,[34] S. Giagu,[51] P. Giannetti,[46] A. Gibson,[28] K. Gibson,[12] C. Ginsburg,[16] N. Giokaris,[14] K. Giolo,[48] M. Giordani,[54] P. Giromini,[18] M. Giunta,[46] G. Giurgiu,[12] V. Glagolev,[14] D. Glenzinski,[16] M. Gold,[37] N. Goldschmidt,[34] J. Goldstein,[42] G. Gomez,[11] G. Gomez-Ceballos,[11] M. Goncharov,[53] O. González,[31] I. Gorelov,[37] A.T. Goshaw,[15] Y. Gotra,[47] K. Goulianos,[50] A. Gresele,[43] M. Griffiths,[29] S. Grinstein,[21] C. Grosso-Pilcher,[13] R.C. Group,[17] U. Grundler,[23] J. Guimaraes da Costa,[21] Z. Gunay-Unalan,[35] C. Haber,[28] S.R. Hahn,[16] K. Hahn,[45] E. Halkiadakis,[52] A. Hamilton,[33] B.-Y. Han,[49] J.Y. Han,[49] R. Handler,[59] F. Happacher,[18] K. Hara,[55] M. Hare,[56] S. Harper,[42] R.F. Harr,[58] R.M. Harris,[16] K. Hatakeyama,[50] J. Hauser,[8] C. Hays,[15] A. Heijboer,[45] B. Heinemann,[29] J. Heinrich,[45] M. Herndon,[59] D. Hidas,[15] C.S. Hill,[10] D. Hirschbuehl,[25] A. Hocker,[16] A. Holloway,[21] S. Hou,[1] M. Houlden,[29] S.-C. Hsu,[9] B.T. Huffman,[42] R.E. Hughes,[39] J. Huston,[35] J. Incandela,[10] G. Introzzi,[46] M. Iori,[51] Y. Ishizawa,[55] A. Ivanov,[7] B. Iyutin,[32] E. James,[16] D. Jang,[52] B. Jayatilaka,[34] D. Jeans,[51] H. Jensen,[16] E.J. Jeon,[27] S. Jindariani,[17] M. Jones,[48] K.K. Joo,[27] S.Y. Jun,[12] T.R. Junk,[23] T. Kamon,[53] J. Kang,[34] P.E. Karchin,[58] Y. Kato,[41] Y. Kemp,[25] R. Kephart,[16] U. Kerzel,[25] V. Khotilovich,[53] B. Kilminster,[39] D.H. Kim,[27] H.S. Kim,[27] J.E. Kim,[27] M.J. Kim,[12] S.B. Kim,[27] S.H. Kim,[55] Y.K. Kim,[13] L. Kirsch,[6] S. Klimenko,[17] M. Klute,[32] B. Knuteson,[32] B.R. Ko,[15] H. Kobayashi,[55] K. Kondo,[57] D.J. Kong,[27] J. Konigsberg,[17] A. Korytov,[17] A.V. Kotwal,[15] A. Kovalev,[45] A. Kraan,[45] J. Kraus,[23] I. Kravchenko,[32] M. Kreps,[25] J. Kroll,[45] N. Krumnack,[4] M. Kruse,[15] V. Krutelyov,[53] S. E. Kuhlmann,[2] Y. Kusakabe,[57] S. Kwang,[13] A.T. Laasanen,[48] S. Lai,[33] S. Lami,[46] S. Lammel,[16] M. Lancaster,[30] R.L. Lander,[7] K. Lannon,[39] A. Lath,[52] G. Latino,[46] I. Lazzizzera,[43] T. LeCompte,[2] J. Lee,[49] J. Lee,[27] Y.J. Lee,[27] S.W. Lee,[53] R. Lefèvre,[3] N. Leonardo,[32] S. Leone,[46] S. Levy,[13] J.D. Lewis,[16] C. Lin,[60] C.S. Lin,[16] M. Lindgren,[16] E. Lipeles,[9] T.M. Liss,[23] A. Lister,[19] D.O. Litvintsev,[16] T. Liu,[16] N.S. Lockyer,[45] A. Loginov,[36] M. Loreti,[43] P. Loverre,[51] R.-S. Lu,[1] D. Lucchesi,[43] P. Lujan,[28] P. Lukens,[16] G. Lungu,[17] L. Lyons,[42] J. Lys,[28] R. Lysak,[1] E. Lytken,[48] P. Mack,[25] D. MacQueen,[33] R. Madrak,[16] K. Maeshima,[16] T. Maki,[22] P. Maksimovic,[24] S. Malde,[42] G. Manca,[29] F. Margaroli,[5] R. Marginean,[16] C. Marino,[23] A. Martin,[60] V. Martin,[38] M. Martínez,[3] T. Maruyama,[55] H. Matsunaga,[55] M.E. Mattson,[58] R. Mazini,[33] P. Mazzanti,[5]

K.S. McFarland,[49] P. McIntyre,[53] R. McNulty,[29] A. Mehta,[29] S. Menzemer,[11] A. Menzione,[46] P. Merkel,[48] C. Mesropian,[50] A. Messina,[51] M. von der Mey,[8] T. Miao,[16] N. Miladinovic,[6] J. Miles,[32] R. Miller,[35] J.S. Miller,[34] C. Mills,[10] M. Milnik,[25] R. Miquel,[28] A. Mitra,[1] G. Mitselmakher,[17] A. Miyamoto,[26] N. Moggi,[5] B. Mohr,[8] R. Moore,[16] M. Morello,[46] P. Movilla Fernandez,[28] J. Mülmenstädt,[28] A. Mukherjee,[16] Th. Muller,[25] R. Mumford,[24] P. Murat,[16] J. Nachtman,[16] J. Naganoma,[57] S. Nahn,[32] I. Nakano,[40] A. Napier,[56] D. Naumov,[37] V. Necula,[17] C. Neu,[45] M.S. Neubauer,[9] J. Nielsen,[28] T. Nigmanov,[47] L. Nodulman,[2] O. Norniella,[3] E. Nurse,[30] T. Ogawa,[57] S.H. Oh,[15] Y.D. Oh,[27] T. Okusawa,[41] R. Oldeman,[29] R. Orava,[22] K. Osterberg,[22] C. Pagliarone,[46] E. Palencia,[11] R. Paoletti,[46] V. Papadimitriou,[16] A.A. Paramonov,[13] B. Parks,[39] S. Pashapour,[33] J. Patrick,[16] G. Pauletta,[54] M. Paulini,[12] C. Paus,[32] D.E. Pellett,[7] A. Penzo,[54] T.J. Phillips,[15] G. Piacentino,[46] J. Piedra,[44] L. Pinera,[17] K. Pitts,[23] C. Plager,[8] L. Pondrom,[59] X. Portell,[3] O. Poukhov,[14] N. Pounder,[42] F. Prakoshyn,[14] A. Pronko,[16] J. Proudfoot,[2] F. Ptohos,[18] G. Punzi,[46] J. Pursley,[24] J. Rademacker,[42] A. Rahaman,[47] A. Rakitin,[32] S. Rappoccio,[21] F. Ratnikov,[52] B. Reisert,[16] V. Rekovic,[37] N. van Remortel,[22] P. Renton,[42] M. Rescigno,[51] S. Richter,[25] F. Rimondi,[5] L. Ristori,[46] W.J. Robertson,[15] A. Robson,[20] T. Rodrigo,[11] E. Rogers,[23] S. Rolli,[56] R. Roser,[16] M. Rossi,[54] R. Rossin,[17] C. Rott,[48] A. Ruiz,[11] J. Russ,[12] V. Rusu,[13] H. Saarikko,[22] S. Sabik,[33] A. Safonov,[53] W.K. Sakumoto,[49] G. Salamanna,[51] O. Saltó,[3] D. Saltzberg,[8] C. Sanchez,[3] L. Santi,[54] S. Sarkar,[51] L. Sartori,[46] K. Sato,[55] P. Savard,[33] A. Savoy-Navarro,[44] T. Scheidle,[25] P. Schlabach,[16] E.E. Schmidt,[16] M.P. Schmidt,[60] M. Schmitt,[38] T. Schwarz,[34] L. Scodellaro,[11] A.L. Scott,[10] A. Scribano,[46] F. Scuri,[46] A. Sedov,[48] S. Seidel,[37] Y. Seiya,[41] A. Semenov,[14] L. Sexton-Kennedy,[16] I. Sfiligoi,[18] M.D. Shapiro,[28] T. Shears,[29] P.F. Shepard,[47] D. Sherman,[21] M. Shimojima,[55] M. Shochet,[13] Y. Shon,[59] I. Shreyber,[36] A. Sidoti,[44] P. Sinervo,[33] A. Sisakyan,[14] J. Sjolin,[42] A. Skiba,[25] A.J. Slaughter,[16] K. Sliwa,[56] J.R. Smith,[7] F.D. Snider,[16] R. Snihur,[33] M. Soderberg,[34] A. Soha,[7] S. Somalwar,[52] V. Sorin,[35] J. Spalding,[16] M. Spezziga,[16] F. Spinella,[46] T. Spreitzer,[33] P. Squillacioti,[46] M. Stanitzki,[60] A. Staveris-Polykalas,[46] R. St. Denis,[20] B. Stelzer,[8] O. Stelzer-Chilton,[42] D. Stentz,[38] J. Strologas,[37] D. Stuart,[10] J.S. Suh,[27] A. Sukhanov,[17] K. Sumorok,[32] H. Sun,[56] T. Suzuki,[55] A. Taffard,[23] R. Takashima,[40] Y. Takeuchi,[55] K. Takikawa,[55] M. Tanaka,[2]

R. Tanaka,[40] N. Tanimoto,[40] M. Tecchio,[34] P.K. Teng,[1] K. Terashi,[50] S. Tether,[32] J. Thom,[16] A.S. Thompson,[20] E. Thomson,[45] P. Tipton,[49] V. Tiwari,[12] S. Tkaczyk,[16] D. Toback,[53] S. Tokar,[14] K. Tollefson,[35] T. Tomura,[55] D. Tonelli,[46] M. Tönnesmann,[35] S. Torre,[18] D. Torretta,[16] S. Tourneur,[44] W. Trischuk,[33] R. Tsuchiya,[57] S. Tsuno,[40] N. Turini,[46] F. Ukegawa,[55] T. Unverhau,[20] S. Uozumi,[55] D. Usynin,[45] A. Vaiciulis,[49] S. Vallecorsa,[19] A. Varganov,[34] E. Vataga,[37] G. Velev,[16] G. Veramendi,[23] V. Veszpremi,[48] R. Vidal,[16] I. Vila,[11] R. Vilar,[11] T. Vine,[30] I. Vollrath,[33] I. Volobouev,[28] G. Volpi,[46] F. Würthwein,[9] P. Wagner,[53] R. G. Wagner,[2] R.L. Wagner,[16] W. Wagner,[25] R. Wallny,[8] T. Walter,[25] Z. Wan,[52] S.M. Wang,[1] A. Warburton,[33] S. Waschke,[20] D. Waters,[30] W.C. Wester III,[16] B. Whitehouse,[56] D. Whiteson,[45] A.B. Wicklund,[2] E. Wicklund,[16] G. Williams,[33] H.H. Williams,[45] P. Wilson,[16] B.L. Winer,[39] P. Wittich,[16] S. Wolbers,[16] C. Wolfe,[13] T. Wright,[34] X. Wu,[19] S.M. Wynne,[29] A. Yagil,[16] K. Yamamoto,[41] J. Yamaoka,[52] T. Yamashita,[40] C. Yang,[60] U.K. Yang,[13] Y.C. Yang,[27] W.M. Yao,[28] G.P. Yeh,[16] J. Yoh,[16] K. Yorita,[13] T. Yoshida,[41] G.B. Yu,[49] I. Yu,[27] S.S. Yu,[16] J.C. Yun,[16] L. Zanello,[51] A. Zanetti,[54] I. Zaw,[21] F. Zetti,[46] X. Zhang,[23] J. Zhou,[52] and S. Zucchelli[5]

(CDF Collaboration)

[1]*Institute of Physics, Academia Sinica, Taipei, Taiwan 11529, Republic of China*

[2]*Argonne National Laboratory, Argonne, Illinois 60439*

[3]*Institut de Fisica d'Altes Energies, Universitat Autonoma de Barcelona, E-08193, Bellaterra (Barcelona), Spain*

[4]*Baylor University, Waco, Texas 76798*

[5]*Istituto Nazionale di Fisica Nucleare, University of Bologna, I-40127 Bologna, Italy*

[6]*Brandeis University, Waltham, Massachusetts 02254*

[7]*University of California, Davis, Davis, California 95616*

[8]*University of California, Los Angeles, Los Angeles, California 90024*

[9]*University of California, San Diego, La Jolla, California 92093*

[10]*University of California, Santa Barbara, Santa Barbara, California 93106*

[11]*Instituto de Fisica de Cantabria, CSIC-University of Cantabria, 39005 Santander, Spain*
[12]*Carnegie Mellon University, Pittsburgh, PA 15213*
[13]*Enrico Fermi Institute, University of Chicago, Chicago, Illinois 60637*
[14]*Joint Institute for Nuclear Research, RU-141980 Dubna, Russia*
[15]*Duke University, Durham, North Carolina 27708*
[16]*Fermi National Accelerator Laboratory, Batavia, Illinois 60510*
[17]*University of Florida, Gainesville, Florida 32611*
[18]*Laboratori Nazionali di Frascati, Istituto Nazionale di Fisica Nucleare, I-00044 Frascati, Italy*
[19]*University of Geneva, CH-1211 Geneva 4, Switzerland*
[20]*Glasgow University, Glasgow G12 8QQ, United Kingdom*
[21]*Harvard University, Cambridge, Massachusetts 02138*
[22]*Division of High Energy Physics, Department of Physics, University of Helsinki and Helsinki Institute of Physics, FIN-00014, Helsinki, Finland*
[23]*University of Illinois, Urbana, Illinois 61801*
[24]*The Johns Hopkins University, Baltimore, Maryland 21218*
[25]*Institut für Experimentelle Kernphysik, Universität Karlsruhe, 76128 Karlsruhe, Germany*
[26]*High Energy Accelerator Research Organization (KEK), Tsukuba, Ibaraki 305, Japan*
[27]*Center for High Energy Physics: Kyungpook National University, Taegu 702-701, Korea; Seoul National University, Seoul 151-742, Korea; and SungKyunKwan University, Suwon 440-746, Korea*
[28]*Ernest Orlando Lawrence Berkeley National Laboratory, Berkeley, California 94720*
[29]*University of Liverpool, Liverpool L69 7ZE, United Kingdom*
[30]*University College London, London WC1E 6BT, United Kingdom*
[31]*Centro de Investigaciones Energeticas Medioambientales y Tecnologicas, E-28040 Madrid, Spain*
[32]*Massachusetts Institute of Technology, Cambridge, Massachusetts 02139*
[33]*Institute of Particle Physics: McGill University, Montréal, Canada H3A 2T8; and University of Toronto, Toronto, Canada M5S 1A7*
[34]*University of Michigan, Ann Arbor, Michigan 48109*
[35]*Michigan State University, East Lansing, Michigan 48824*

[36]*Institution for Theoretical and Experimental Physics, ITEP, Moscow 117259, Russia*
[37]*University of New Mexico, Albuquerque, New Mexico 87131*
[38]*Northwestern University, Evanston, Illinois 60208*
[39]*The Ohio State University, Columbus, Ohio 43210*
[40]*Okayama University, Okayama 700-8530, Japan*
[41]*Osaka City University, Osaka 588, Japan*
[42]*University of Oxford, Oxford OX1 3RH, United Kingdom*
[43]*University of Padova, Istituto Nazionale di Fisica Nucleare, Sezione di Padova-Trento, I-35131 Padova, Italy*
[44]*LPNHE, Universite Pierre et Marie Curie/IN2P3-CNRS, UMR7585, Paris, F-75252 France*
[45]*University of Pennsylvania, Philadelphia, Pennsylvania 19104*
[46]*Istituto Nazionale di Fisica Nucleare Pisa, Universities of Pisa, Siena and Scuola Normale Superiore, I-56127 Pisa, Italy*
[47]*University of Pittsburgh, Pittsburgh, Pennsylvania 15260*
[48]*Purdue University, West Lafayette, Indiana 47907*
[49]*University of Rochester, Rochester, New York 14627*
[50]*The Rockefeller University, New York, New York 10021*
[51]*Istituto Nazionale di Fisica Nucleare, Sezione di Roma 1, University of Rome "La Sapienza," I-00185 Roma, Italy*
[52]*Rutgers University, Piscataway, New Jersey 08855*
[53]*Texas A&M University, College Station, Texas 77843*
[54]*Istituto Nazionale di Fisica Nucleare, University of Trieste/ Udine, Italy*
[55]*University of Tsukuba, Tsukuba, Ibaraki 305, Japan*
[56]*Tufts University, Medford, Massachusetts 02155*
[57]*Waseda University, Tokyo 169, Japan*
[58]*Wayne State University, Detroit, Michigan 48201*
[59]*University of Wisconsin, Madison, Wisconsin 53706*
[60]*Yale University, New Haven, Connecticut 06520*

Abstract

We present a measurement of the B_c^+ meson lifetime in the semileptonic decay mode $B_c^+ \rightarrow J/\psi e^+ \nu_e$ using the CDF II detector at the Fermilab Tevatron Collider. From a sample of about 360 pb^{-1} of p$\bar{\text{p}}$ collisions at $\sqrt{s} = 1.96$ TeV, we reconstruct $J/\psi e^+$ pairs with invariant mass in the kinematically allowed range $4 < M_{J/\psi e} < 6\,\text{GeV}/c^2$. A fit to the decay-length distribution of 238 signal events yields a measured B_c^+ meson lifetime of $0.463\ ^{+0.073}_{-0.065}\ (stat) \pm 0.036\ (syst)$ ps.

PACS numbers: 13.20.He, 14.40.Nd

The B_c^+ meson is the only known meson consisting of two heavy quarks of different flavor: a charm quark and a bottom antiquark. It provides a unique test of heavy-quark dynamics, since the bound state can be treated using the same non-relativistic expansion that successfully describes both $c\bar{c}$ and $b\bar{b}$ families. However, unlike $c\bar{c}$ and $b\bar{b}$ states, the B_c^+ meson decays only via weak interactions, thus having a measurable lifetime. The lifetime of the B_c^+ meson is expected to be about two to three times smaller than the B^+ meson lifetime if one assumes three major decay subprocesses [1, 2]: $\bar{b}$ quark decay with c quark as spectator, c quark decay with $\bar{b}$ quark as spectator, and $\bar{b}c$ annihilation decays. An early measurement from CDF [3] found a lifetime consistent with predictions. More precise measurements will determine the relative importance of the three decay subprocesses and provide insight into the strong dynamics of heavy quarks. In this Letter, we report a new B_c^+ meson lifetime measurement using the decay mode $B_c^+ \to J/\psi e^+ \nu_e$. Charge-conjugate modes are implied throughout this Letter. The new measurement is about 2.5 times more precise than the previous one.

We use a data sample of about 360 pb^{-1} collected between February 2002 and August 2004 with the CDF II detector [4] at the Fermilab Tevatron Collider at a center of mass energy of 1.96 TeV. The components of the CDF II detector pertinent to this analysis are briefly described below. A cylindrical drift chamber (COT) [5] and a silicon microstrip detector [6] immersed in a 1.4 T solenoidal magnetic field track charged particles in the pseudorapidity range $|\eta| < 1$ [7]. The COT has 96 measurement layers, between 40 and 137 cm in radius, organized into alternating axial and stereo superlayers. Seven layers of double-sided silicon sensors provide precise position measurements at radii between 2.5 and 28 cm. Four layers of planar drift chambers (CMU) [8] detect muons with momentum transverse to the beam line $p_T > 1.4\,\mathrm{GeV}/c$ within $|\eta| < 0.6$. Conical sections of drift tubes [9] cover $0.6 < |\eta| < 1.0$ for muons with $p_T > 2\,\mathrm{GeV}/c$. A lead-scintillator calorimeter (CEM) [10] provides electron identification for $|\eta| < 1.1$. An embedded multiwire proportional chamber (CES) located near shower maximum at about six radiation lengths and a preshower wire chamber (CPR) between the magnet coil and the CEM located at about one radiation length provide fine-grained measurements of the longitudinal and transverse shower development.

The $B_c^+ \to J/\psi e^+ \nu_e$ reconstruction starts with $J/\psi \to \mu^+\mu^-$ candidates collected by the CDF di-muon triggers [4, 11], where at least one muon is required to be detected in the CMU. The J/ψ candidates are further purified during offline reconstruction by vertex constraining

the $\mu^+\mu^-$ pairs and by selecting the pairs with transverse momentum $p_{T_{J/\psi}} > 3\,\mathrm{GeV}/c$. Then, each J/ψ candidate with a reconstructed mass within $50\,\mathrm{MeV}/c^2$ of its nominal value is combined with an electron to form a B_c^+ candidate.

Electron identification uses both specific ionization (dE/dx) information from the COT and calorimeter shower information from the CEM, CES, and CPR. The logarithm of the ratio of the measured dE/dx value from a charged particle to that expected for an electron, $Z_e = \log(dE/dx) - \log(dE/dx)_{\mathrm{predict}}$, is compared to its standard deviation σ_{Z_e}. The expected dE/dx and σ_{Z_e} are functions of the particle charge, momentum, and the multiplicity of associated COT hits. Electron candidates are required to have $Z_e/\sigma_{Z_e} > -1.3$ to reject hadrons ($\pi/K/p$) while remaining efficient for true electrons. Enriched samples of electrons, pions, kaons, and protons are used to determine the dE/dx identification efficiencies listed in Table I. The enriched samples come from photon conversions, $\gamma \to e^+e^-$, and from hadron decays, $K_s^0 \to \pi^+\pi^-$, $D^0 \to K^-\pi^+$, and $\Lambda^0 \to p\pi^-$. The hadrons surviving the Z_e/σ_{Z_e} cut are dominated by pions, which are rejected by comparing their calorimeter shower shapes to those of electrons. Charged particles with $p_T > 2\,\mathrm{GeV}/c$ are extrapolated into the calorimeter to match shower clusters in the CEM, CES, and CPR. The probabilities for a particle to have a shower shape consistent with being an electron or a hadron are calculated using the distributions of shower energy and shower cluster profiles for the enriched electron and hadron samples described above. We first define a ratio of probability for a charged particle to be an electron as the ratio between its joint probability to be an electron and the sum of its probabilities to be an electron or a hadron. We then obtain a cumulative probability distribution of the ratio using the enriched electron sample and impose a cut on electron candidates at a 70% probability value. To calculate the average probability for hadrons to pass this requirement, we use enriched hadron samples having $Z_e/\sigma_{Z_e} > -1.3$ in a mix of $\pi/K/p$ particles predicted by a PYTHIA Monte Carlo simulation of $B \to J/\psi X$ events [12]. This averaged probability as a function of p_T is listed in Table I. Overall, the electron identification using combined dE/dx and calorimeter information has an efficiency of 60% for true electrons, while hadrons have a probability to pass the selection lower than 0.15%. Electrons found to originate from photon conversion, $\gamma \to e^+e^-$, are removed from consideration as $J/\psi e^+$ candidates.

A B_c^+ candidate is a $J/\psi e^+$ pair with transverse momentum $p_{T_{J/\psi e}} > 5\,\mathrm{GeV}/c$ and invariant mass $4 < M_{J/\psi e} < 6\,\mathrm{GeV}/c^2$. The lower bound on $M_{J/\psi e}$ is set higher than the

TABLE I: Electron identification efficiencies (%) as functions of particle p_T (GeV/c) using dE/dx and calorimeter (Cal) for electron and hadrons. The dE/dx results are averages of positively and negatively charged particles. The calorimeter results for hadrons (h) are the weighted averages of π, K and p. The conversion-finding efficiency ϵ_{conv} is also listed.

p_T	2-3	3-4	4-5	5-6	> 6
dE/dx:e	91.3 ± 0.1	91.4 ± 0.2	90.7 ± 0.2	90.5 ± 0.3	89.5 ± 0.2
dE/dx:π	16.4 ± 0.1	23.8 ± 0.1	32.0 ± 0.1	39.0 ± 0.2	49.4 ± 0.2
dE/dx:K	2.09 ± 0.09	2.35 ± 0.07	3.29 ± 0.09	4.4 ± 0.1	9.5 ± 0.2
dE/dx:p	3.38 ± 0.03	2.14 ± 0.04	2.54 ± 0.07	3.0 ± 0.1	4.9 ± 0.2
Cal:e^+	68.5 ± 0.3	68.8 ± 0.5	68.9 ± 0.8	68.9 ± 1.1	67.6 ± 1.0
Cal:e^-	67.9 ± 0.4	69.5 ± 0.5	69.6 ± 0.7	68.1 ± 1.2	68.5 ± 0.9
Cal:h^+	0.77 ± 0.04	0.37 ± 0.04	0.37 ± 0.03	0.29 ± 0.04	0.13 ± 0.04
Cal:h^-	0.64 ± 0.04	0.37 ± 0.02	0.27 ± 0.03	0.25 ± 0.04	0.21 ± 0.04
ϵ_{conv}	49.8 ± 1.4	55.0 ± 2.2	56.5 ± 3.3	61.5 ± 4.5	69.2 ± 3.4

kinematic limit of $M_{J/\psi}$ to reduce the background from B_c^+ semileptonic decays other than the exclusive decay $B_c^+ \to J/\psi e^+ \nu_e$ to a few percent [1, 3]. The opening angle between the J/ψ and electron momenta must satisfy $\Delta\phi < 90°$ to reduce generic $b\bar{b}$ background that produces a J/ψ and an electron from different b hadrons. Finally, the tracks of the three daughter particles, μ^+, μ^-, and e^+, are fit to a common vertex and the fit probability is required to exceed 0.1%. The B_c^+ decay length in the transverse plane, L_{xy}, is calculated as the projection of the displacement of the B_c^+ vertex from the primary vertex onto the momentum of the $J/\psi e^+$ system. The primary vertex position is obtained from run-by-run averages using samples of prompt tracks.

Before making a lifetime measurement, we first establish the B_c^+ signal in the $J/\psi e^+$ pairs. The background pairs from prompt decays are removed here by imposing a selection of $L_{xy}/\sigma_{L_{xy}} > 3$. The $M_{J/\psi e}$ distribution from $J/\psi e^+$ pairs passing the $L_{xy}/\sigma_{L_{xy}}$ cut is shown in Fig.1. Within the $4 < M_{J/\psi e} < 6\,\mathrm{GeV}/c^2$ window, 203 candidates are found with a background of 88 ± 14 from fake J/ψ, fake electrons from hadrons, photon conversion electrons, and decays resulting from $b\bar{b}$, as listed in Table II. The number of fake J/ψ candidates from combinatorial background is estimated using $\mu^+\mu^-$ pairs with invariant mass

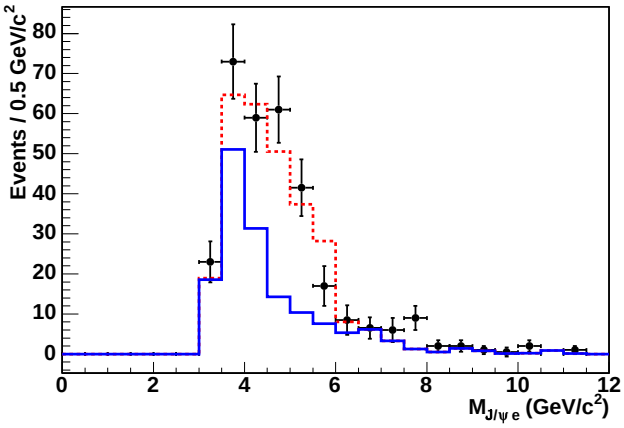

FIG. 1: Invariant mass distribution of the $J/\psi e^+$ pairs with $L_{xy}/\sigma_{L_{xy}} > 3$ (data with error bars) together with predicted mass shape (dashed line) from a sum of a Monte Carlo simulation for signal and estimated background (solid lines). The contributions from fake J/ψ are already subtracted.

outside the $50\,\mathrm{MeV}/c^2$ window for J/ψ candidates. To estimate the hadron backgrounds, we use a sample of J/ψ-track pairs passing the same selection criteria as the $J/\psi e^+$ pairs, including the dE/dx requirement and the requirement to point to the CEM fiducial region, but without any selection based on calorimeter information. The size of the contribution is estimated from a weighted counting of the J/ψ-track pairs with the weights taken as the averaged probabilities in Table I for hadrons to pass the electron selection criteria using the calorimeter. We derive the residual conversion electron contribution from the rate of identified photon conversions together with the conversion-finding efficiency listed in Table I. The conversion-finding efficiency, defined as the fraction of the identified electrons with their conversion partners in the kinematic acceptance of the CDF detector, is estimated from a Monte Carlo simulation. Finally, the contribution from decays resulting from $b\bar{b}$ production is estimated using a PYTHIA Monte Carlo sample with relative rates of flavor creation, flavor excitation, and gluon splitting tuned from data [12, 13]. The number of B_c^+ signal events is found to be 115 ± 16 $(stat) \pm 14$ $(syst)$. For comparison, there are 2872 ± 59 $B^+ \to J/\psi K^+$ signal events in the data sample corresponding to the same integrated luminosity. We find the production rate of B_c^+ relative to that of B^+, $[\sigma(B_c^+) \cdot \mathcal{B}(B_c^+ \to J/\psi e^+ \nu_e)]/[\sigma(B^+) \cdot \mathcal{B}(B^+ \to J/\psi K^+)]$, in the kinematic range $p_T > 4\,\mathrm{GeV}/c$ and rapidity $|y| < 1$ to be 0.282 ± 0.038 $(stat) \pm 0.035$ $(syst) \pm 0.065$ $(acceptance)$. The first error is statistical; the second covers the systematic uncertainty of B_c^+ signal excess counting, and the third pertains

to the estimated detector acceptance ratio correction $A_{B^+}/A_{B_c^+} = 4.42 \pm 1.02$ from Monte Carlo simulation where the B_c^+ p_T spectrum, its lifetime values and decay modes are the major sources of uncertainty. This new production ratio result agrees well with the earlier CDF measurement [3].

TABLE II: Numbers of observed $J/\psi e^+$ pairs with $4 < M_{J/\psi e} < 6\,\mathrm{GeV}/c^2$ and estimated backgrounds. The error listed contains both the statistical and systematic errors.

	No L_{xy} cut	$L_{xy}/\sigma_{L_{xy}} > 3$
fake J/ψ	164.0 ± 9.1	24.5 ± 3.5
fake electron	110.2 ± 19.0	15.4 ± 2.5
conversion electron	67.4 ± 34.8	14.5 ± 7.8
$b\bar{b}$	63.0 ± 18.5	33.6 ± 11.4
prompt decay	141.7 ± 32.0	-
total background	545 ± 55	88 ± 14
observed $J/\psi e^+$ pairs	783	203

Having established a clear B_c^+ signal in $J/\psi e^+$ combinations, we measure the B_c^+ meson lifetime in a larger sample of 783 $J/\psi e^+$ events, selected with the same criteria as above, but without the L_{xy} cut or fake J/ψ subtraction. We estimate the net signal excess in this sample to be 238. The background sources and their contributions are listed in Table II. Contributions from fake electrons, conversion electrons, $b\bar{b}$ decays, and fake J/ψ are estimated as described earlier. The number of additional prompt-decay events is extracted directly from the lifetime fit.

An unbinned maximum-likelihood fit is used to extract the B_c^+ meson lifetime. The transverse decay length L_{xy} and its event-by-event error $\sigma_{L_{xy}}$ from the $J/\psi e^+$ pairs are the input variables for the fit. The lifetime fitting likelihood function has the form [14]

$$\begin{aligned}\mathcal{F}(L_{xy}, \sigma_{L_{xy}}) &= (1 - \sum_1^5 f_{b_i})\mathcal{F}_s(L_{xy}, \sigma_{L_{xy}})\mathcal{P}_s(\sigma_{L_{xy}}) \\ &+ \sum_1^5 f_{b_i}\mathcal{F}_{b_i}(L_{xy}, \sigma_{L_{xy}})\mathcal{P}_{b_i}(\sigma_{L_{xy}}), \end{aligned} \quad (1)$$

where $\mathcal{F}_s(L_{xy}, \sigma_{L_{xy}})$ is the lifetime Probability Distribution Function (PDF) for pure B_c^+ signal, f_{b_i} and $\mathcal{F}_{b_i}(L_{xy}, \sigma_{L_{xy}})$ are fractions of the five background contributions and their

lifetime PDFs, and $\mathcal{P}_s(\sigma_{L_{xy}})$ and $\mathcal{P}_{b_i}(\sigma_{L_{xy}})$ are the PDFs of the $\sigma_{L_{xy}}$ for signal and backgrounds. The lifetime PDF for the B_c^+ signal, $\mathcal{F}_s(L_{xy}, \sigma_{L_{xy}})$, is assumed to be an exponential lifetime distribution convoluted with a Gaussian resolution function. In the calculation, the transverse decay length is related to the Lorentz-invariant proper decay time by a Lorentz boost $\beta_{\mathrm{T}}\gamma = p_{T_{B_c}}/M_{B_c} = (p_{T_{J/\psi e}}/M_{J/\psi e}) \cdot \cos\alpha/K$, where where α is the angle between the vectors of $p_{T_{J/\psi e}}$ and $p_{T_{B_c}}$. The B_c^+ mass M_{B_c} is assumed to have a value of 6.271 GeV/c^2 [2] in the calculation. The transverse momentum of the B_c^+, $p_{T_{B_c}}$, is calculated from $p_{T_{J/\psi e}}$ with a correction $K \equiv (p_{T_{J/\psi e}}/p_{T_{B_c}}) \cdot (M_{B_c}/M_{J/\psi e}) \cdot \cos\alpha$. The K distributions, shown in Fig.2, are obtained from a Monte Carlo calculation for four $M_{J/\psi e}$ bins. For background $\mathcal{F}_{b_i}(L_{xy}, \sigma_{L_{xy}})$ calculation, the variable before correction, $L_{xy}M_{J/\psi e}/p_{T_{J/\psi e}}$, called pseudo-proper decay time, is used directly. The prompt background is assumed to have zero lifetime with a Gaussian resolution function. Other backgrounds are described by a sum of a Gaussian distribution centered at zero and two pairs of positive and negative exponential lifetime functions. The initial parameters for these background PDFs are obtained from fits to the background samples as shown in Fig. 3. The obtained results are used to constrain the corresponding parameters in the final lifetime fit. The constraints are imposed by multiplying the likelihood function with Gaussian functions of the appropriate mean and width. Similarly, the background fractions f_{b_i} are also constrained during the B_c^+ meson lifetime fit.

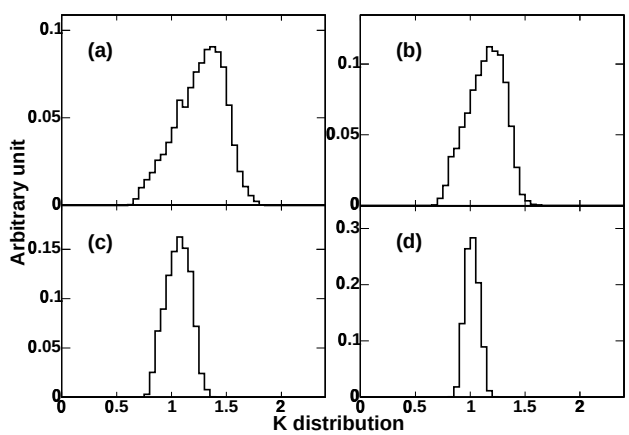

FIG. 2: Distribution of K from Monte Carlo simulation for four $M_{J/\psi e}$ bins, (a) 4-4.5 GeV/c^2, (b) 4.5-5.0 GeV/c^2, (c) 5.0-5.5 GeV/c^2 and (d) 5.5-6.0 GeV/c^2.

In Fig.4, the pseudo-proper decay time distribution from the 783 B_c^+ candidates is shown

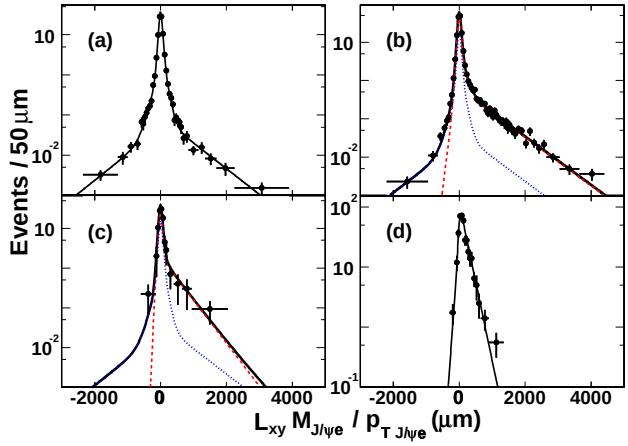

FIG. 3: Fit results of background PDFs for (a) fake J/ψ (solid lines), (b) fake electron (dashed lines), (c) conversion electron (dashed lines) and (d) $b\bar{b}$ decays (solid lines). For (b) and (c), the fake J/ψ contributions and shapes (dotted lines) are constrained to that obtained from sideband events. The $b\bar{b}$ background events for (d) are from Monte Carlo simulation.

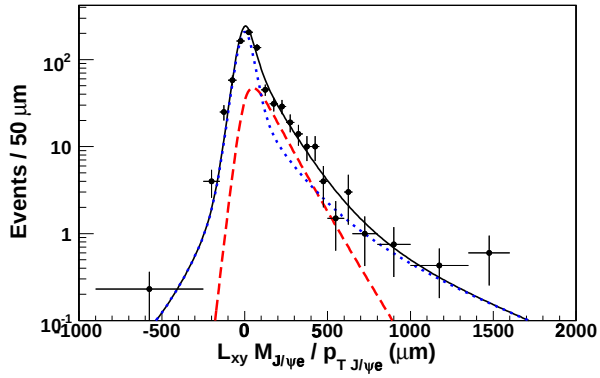

FIG. 4: Pseudo-proper decay time distribution from 783 B_c^+ candidates. The points with error bars are data points and the solid line is the fit result. The dashed line is the B_c^+ signal distribution and the dotted line is the background contribution.

together with the fitting result superimposed. We find $c\tau_{B_c} = 139^{+22}_{-20}$ μm. The sources of systematic uncertainty on the lifetime fit are now considered, and their magnitudes are estimated. The uncertainty associated with the K distribution is estimated by varying the p_T spectrum, the mass and lifetime values, and the B_c^+ meson decay modes used in the Monte Carlo. The p_T spectrum is varied from using a theoretical calculation [15] for B_c^+ production to that of the inclusive decay $B \to J/\psi X$ [4]. The mass and lifetime in the

Monte Carlo are varied in the ranges $M_{B_c} = 6.2 - 6.4$ GeV/c^2 and $\tau_{B_c} = 0.4 - 0.7$ ps [1, 2]. The B_c^+ semileptonic decay considered in the simulation is varied from the exclusive $B_c^+ \to J/\psi e^+ \nu_e$ alone to that of an inclusive decay table predicted in Ref. [1]. The effect of the K distribution uncertainty on the B_c^+ lifetime fit is estimated to be $\Delta c\tau_{B_c} = \pm 2.8$ μm by using variations of the K distributions. The uncertainty related to background lifetime shapes is estimated from investigating the p_T dependence of the electron identification efficiencies and the conversion-finding efficiency, from using fake J/ψ events from different samples, and from changing fractions of $b\bar{b}$ events originating from the three main mechanisms according to a fit using CDF data [13]. The estimated effect from background shape uncertainties is ± 9.2 μm. Finally, the uncertainty related to the L_{xy} calculation and its error distribution is found to be ± 4.7 μm from the uncertainty in the silicon detector alignment, by using an alternative resolution functional form to include additional Gaussian and symmetric exponential tails, and by using alternative decay-length error distributions. Adding all the estimated systematic errors in quadrature we find $c\tau_{B_c} = 139\ ^{+22}_{-20}\ (stat) \pm 11\ (syst)$ μm or $\tau_{B_c} = 0.463\ ^{+0.073}_{-0.065}\ (stat) \pm 0.036\ (syst)$ ps.

In conclusion, from an unbinned maximum-likelihood fit to the decay-length distribution of 238 signal events of $B_c^+ \to J/\psi e^+ \nu_e$, the B_c^+ meson lifetime is found to be $0.463\ ^{+0.073}_{-0.065}\ (stat) \pm 0.036\ (syst)$ ps which is about one third of the B^+ meson lifetime. This agrees with theoretical models [1, 2] in which all the three major decay subprocesses, the two spectator processes ($\bar{b}$-quark and c-quark) and the $\bar{b}c$ annihilation, play important roles in the B_c^+ decays.

We thank the Fermilab staff and the technical staffs of the participating institutions for their vital contributions. This work was supported by the U.S. Department of Energy and National Science Foundation; the Italian Istituto Nazionale di Fisica Nucleare; the Ministry of Education, Culture, Sports, Science and Technology of Japan; the Natural Sciences and Engineering Research Council of Canada; the National Science Council of the Republic of China; the Swiss National Science Foundation; the A.P. Sloan Foundation; the Bundesministerium für Bildung und Forschung, Germany; the Korean Science and Engineering Foundation and the Korean Research Foundation; the Particle Physics and Astronomy Research Council and the Royal Society, UK; the Russian Foundation for Basic Research; the Comisión Interministerial de Ciencia y Tecnología, Spain; in part by the European Community's Human Potential Programme under contract HPRN-CT-2002-00292; and the

Academy of Finland.

---

[1] V.V.Kiselev, "Decay of the B_c meson", hep-ph/0308214 (21 Aug 2003).

[2] S. Godfrey, Phys. Rev. D **70**, 054017 (2004).

[3] F. Abe *et al.* (CDF Collaboration), Phys. Rev. D **58**, 112004 (1998);
F. Abe *et al.* (CDF Collaboration), Phys. Rev. Lett. **81**, 2432 (1998).

[4] D. Acosta *et al.* (CDF Collaboration), Phys. Rev. D **71**, 032001 (2005).

[5] T. Affolder *et al.*, Nucl. Instrum. Methods. A **526**, 249 (2004).

[6] A. Sill *et al.*, Nucl. Instrum. Methods. A **447**, 1 (2000).

[7] The positive z axis lies along the proton direction, r is the radius from this axis, θ is the polar angle and ϕ is the azimuthal angle. The pseudorapidity is defined as $\eta = -\ln[\tan(\theta/2)]$.

[8] G. Ascoli *et al.*, Nucl. Instrum. Methods. A **268**, 33 (1988).

[9] T. Dorigo *et al.*, Nucl. Instrum. Methods. A **461**, 560 (2001).

[10] L. Balka *et al.*, Nucl. Instrum. Methods. A **267**, 272 (1998);
A. Byon-Wagner *et al.*, IEEE Trans. Nucl. Sci. **49**. 2567 (2002).

[11] E. J. Thomson *et al.*, IEEE Trans. Nucl. Sci. **49**, 1063 (2002);
D. Acosta *et al.* (CDF Collaboration), FERMILAB-PUB-05/535-E (submitted to Phys. Rev. Lett.).

[12] T. Sjostrand and M. Bengtsson, Comput. Phys. Commun. **43**, 367 (1987);
H. U. Bengtsson and T. Sjostrand, Comput. Phys. Commun. **46**, 43 (1987);
R. Field, Phys. Rev. D **65**, 094006 (2002).

[13] D. Acosta *et al.* (CDF Collaboration), Phys. Rev. D **71**, 092001 (2005).

[14] G. Punzi, "Comments on likelihood fits with variable resolution", eConf **C030908**, WELT002 (2003), [arXiv:physics/0401045].

[15] C. H. Chang *et al.*, Comput. Phys. Commun. 159 (2004) 192;
C. H. Chang and X. G. Wu, Eur. Phys. J. C. 38 (2004) 267.